Three-dimensional organization of nascent rod outer segment disk membranes

Stefanie Volland[a], Louise C. Hughes[a,b,c,1], Christina Kong[a], Barry L. Burgess[a], Kenneth A. Linberg[d], Gabriel Luna[d], Z. Hong Zhou[b,c,e], Steven K. Fisher[d,f], and David S. Williams[a,e,g,h,2]

[a]Department of Ophthalmology and Stein Eye Institute, University of California, Los Angeles, CA 90095; [b]Department of Microbiology, Immunology, and Molecular Genetics, University of California, Los Angeles, CA 90095; [c]Electron Imaging Center for Nanoscience, California NanoSystems Institute, University of California, Los Angeles, CA 90095; [d]Neuroscience Research Institute, University of California, Santa Barbara, CA 93106; [e]Molecular Biology Institute, University of California, Los Angeles, CA 90095; [f]Department of Molecular, Cellular, and Developmental Biology, University of California, Santa Barbara, CA 93106; [g]Department of Neurobiology, David Geffen School of Medicine at UCLA, University of California, Los Angeles, CA 90095; and [h]Brain Research Institute, University of California, Los Angeles, CA 90095

Edited by John E. Dowling, Harvard University, Cambridge, MA, and approved October 27, 2015 (received for review August 17, 2015)

The vertebrate photoreceptor cell contains an elaborate cilium that includes a stack of phototransductive membrane disks. The disk membranes are continually renewed, but how new disks are formed remains poorly understood. Here we used electron microscope tomography to obtain 3D visualization of the nascent disks of rod photoreceptors in three mammalian species, to gain insight into the process of disk morphogenesis. We observed that nascent disks are invariably continuous with the ciliary plasma membrane, although, owing to partial enclosure, they can appear to be internal in 2D profiles. Tomographic analyses of the basal-most region of the outer segment show changes in shape of the ciliary plasma membrane indicating an invagination, which is likely a first step in disk formation. The invagination flattens to create the proximal surface of an evaginating lamella, as well as membrane protrusions that extend between adjacent lamellae, thereby initiating a disk rim. Immediately distal to this initiation site, lamellae of increasing diameter are evident, indicating growth outward from the cilium. In agreement with a previous model, our data indicate that mature disks are formed once lamellae reach full diameter, and the growth of a rim encloses the space between adjacent surfaces of two lamellae. This study provides 3D data of nascent and mature rod photoreceptor disk membranes at unprecedented *z*-axis depth and resolution, and provides a basis for addressing fundamental questions, ranging from protein sorting in the photoreceptor cilium to photoreceptor electrophysiology.

photoreceptor | cilium | EM tomography | disk morphogenesis

Primary cilia detect extracellular signals via membrane receptors or channels. The most elaborate of all cilia, the cilium that forms the vertebrate photoreceptor outer segment (OS), includes a large stack of membrane disks that extends distally from the transition zone, also known as the connecting cilium (1). The OS disks contain the visual receptor, opsin, and their tight packing allows for a high concentration of opsin within a confined space, thereby limiting the trade-off between visual sensitivity and spatial resolution. Turnover of OS disk membranes occurs throughout the lifetime of an animal (2) and requires the de novo synthesis and degradation of large amounts of OS proteins; on average, 9–10 billion opsin molecules are turned over every second in each human retina (3).

A key event in OS disk turnover is the formation of disk membranes from newly synthesized molecules that are trafficked as vesicles from the endoplasmic reticulum (ER)/Golgi in the inner segment to the cilium (4, 5). Disk membrane morphogenesis is essential for the survival of photoreceptor cells. Orthologs of gene mutations that disrupt disk formation in mice have been linked to various retinal degenerations in humans; for example, in the *rds* mouse [mutant in peripherin-2 (*Prph2*)], disks do not develop from the end of the connecting cilium (6, 7), and in mice whose photoreceptors express mutant human prominin-1 (*PROM1*), the disks that do form are disorganized (8). *PRPH2* and *PROM1* genes have been linked to different forms of retinitis pigmentosa, macular dystrophy, and cone-rod dystrophy (https://sph.uth.edu/retnet/disease.htm).

Disk membrane morphogenesis clearly involves extensive membrane growth and shaping; however, the process by which these events occur remains largely unresolved. Although there is agreement that mature rod OS disks appear discrete and enclosed entirely by the plasma membrane, models differ fundamentally according to whether the nascent disks form from the ciliary plasma membrane or from the expansion of endosomal membrane. Differences stem from interpretation of whether the nascent disks are open to the extracellular space (9, 10), or closed from it, like the mature disks (11). Whether the nascent disks are open or closed also has important implications for understanding questions of photoreceptor cell biology and electrophysiology, such as how membrane proteins are sorted into the subdomains of the OS (12) and the origin of the early receptor potential (13).

There are several possible reasons for the different interpretations of whether nascent rod disks are open or closed, including differences in tissue preservation methods, species studied, and perhaps the time of day when the retinas were fixed. In an attempt to resolve this discrepancy, we addressed these variables in the present study. Importantly, we also addressed a limitation of

Significance

A vertebrate photoreceptor cell depends on the elaboration of its cilium to generate its light-sensitive organelle, the outer segment (OS), which is made up of a stack of membrane disks, containing the visual receptor, opsin. How this elaboration occurs has been the subject of recent controversy. Here we used electron microscope tomography to obtain a 3D analysis of the membrane organization at the base of the OS, where new membrane disks are continually made to replace the older ones. We show that the nascent disk membrane is continuous with the ciliary plasma membrane, and appears to form by a complex reshaping of this membrane, involving an invagination, followed by outward growth, and, finally, the completion of a disk rim.

Author contributions: S.V., S.K.F., and D.S.W. designed research; S.V., L.C.H., C.K., B.L.B., K.A.L., and G.L. performed research; Z.H.Z. contributed new reagents/analytic tools; S.V., L.C.H., Z.H.Z., S.K.F., and D.S.W. analyzed data; and S.V., S.K.F., and D.S.W. wrote the paper.

The authors declare no conflict of interest.

This article is a PNAS Direct Submission.

[1]Present address: Department of Biological and Medical Sciences, Oxford Brookes University, Oxford OX3 0BP, United Kingdom.

[2]To whom correspondence should be addressed. Email: dswilliams@ucla.edu.

This article contains supporting information online at www.pnas.org/lookup/suppl/doi:10.1073/pnas.1516309112/-/DCSupplemental.

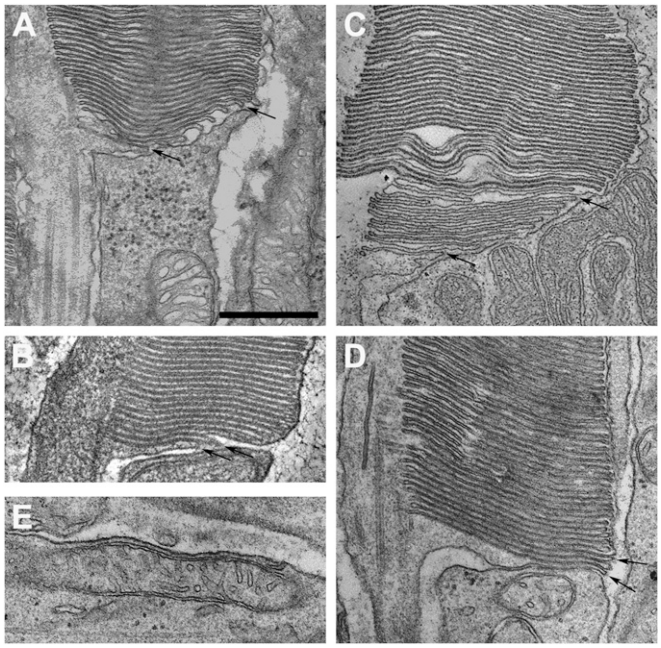

Fig. 1. Fixation of disk membrane morphology. (*A* and *B*) Transmission electron micrographs of the basal disks of mouse rod OSs, preserved by transcardiac perfusion with Karnovsky's fixative and conventional processing (*A*) or by brief transcardiac perfusion with Karnovsky's fixative, followed by HPF-FS (*B*). (*C* and *D*) Transmission electron micrographs of the basal disks of monkey (*C*) and cat (*D*) rod OSs, preserved by transcardiac perfusion with Karnovsky's fixative and conventional processing. In *A–D*, the basal-most disks appear to be open to the extracellular space (and thus are lamellae), as indicated by arrows. (*E*) A typical elongated, well-preserved mitochondrion from the inner segment (adjacent to the basal OS disks) from a cat rod. (Scale bar: 500 nm.) *A–E* are at the same magnification. *B* and *C* are *z*-slices from tomograms; other panels are from transmission electron micrographs of 70-nm sections.

previous studies, the reliance on 2D conventional transmission electron microscopy (TEM), by using TEM tomography (ET) to generate, to our knowledge, the first substantial high-resolution 3D reconstruction of the nascent disks of single rod photoreceptor cells.

Our 3D analysis illustrates that nascent disks consistently have continuities with the ciliary plasma membrane, supporting a model in which their morphogenesis occurs by amplification of this membrane. However, our analysis also demonstrates a previously unappreciated feature of nascent disk organization, and provides insight into the first stages of disk morphogenesis.

Results

Preservation of Disk Membranes. Mouse photoreceptor OSs are notoriously difficult to preserve for TEM, perhaps owing in part to their very high packing density, which for most of the retina is three to four times greater than the photoreceptor density in the human macula (14), and may impede the penetration of fixative. Nascent disk membranes may be especially labile given their transient state, so that variations in the quality of preservation may be responsible for differing reports as to whether the nascent disks in mouse rods are open (15) or closed (16, 17).

Cardiac perfusion with Karnovsky's fixative resulted in well-organized OS disk membranes (Fig. 1*A*), significantly better than when an opened eyecup was simply immersed in the same fixative. Mitochondria (a sensitive indicator of fixation quality) were also well preserved in the apical inner segment.

In addition, we tested the use of high-pressure freezing followed by freeze substitution (HPF-FS). Because the retina is not immediately accessible, HPF-FS could be performed only after dissection of the eye and preparation of small retinal pieces. To avoid possible artifacts during dissection, we preceded dissection with a brief period of cardiac perfusion with Karnovsky's fixative. Previous reports have shown that aldehyde fixation before HPF-FS provides results similar to those from preservation by HPF-FS alone (18). This approach generated a well-preserved photoreceptor ultrastructure, with disk membranes with linear, parallel profiles (Fig. 1*B*).

Fixation by cardiac perfusion of larger mammals resulted in high-quality preservation of OS disks and the photoreceptor mitochondria (Fig. 1 *C–E*). Of note, we observed basal nascent disks that were continuous with the plasma membrane, regardless of species (arrows in Fig. 1 *A–D*).

ET of Nascent Disk Membranes. ET was performed on 300-nm sections. A tomogram of the basal OS of a mouse rod, preserved by HPF-FS, and a 3D model from this tomogram are shown in Movies S1 and S2. In some cases, to increase *z*-axis depth so that it included most of the rod OS diameter, tomograms from serial 300-nm sections were joined along the *z*-axis. From the resulting large tomogram, we observed some *z*-plane images of rod OSs from mouse, cat, and monkey retinas in which the basal disks appeared closed (e.g., Fig. 2 *A* and *E*). Invariably, however, these basal disks were observed to be continuous with the plasma membrane in other *z*-planes; that is, the disks had an opening to the extracellular space. This is demonstrated in Fig. 2 *A–C*, which shows four basal-most disks of a monkey rod in different *z*-planes. In the *z*-plane illustrated in Fig. 2*A*, the red arrow indicates the four appearing as isolated internal structures; note that indentations of the plasma membrane occur opposite each of these. In the plane shown in Fig. 2*B*, the internal disks and the indentations of the plasma membrane are closer together (blue arrow), and in the *z*-plane shown in Fig. 2*C* they are joined, so that the disks are continuous with the plasma membrane, demonstrating that they are actually lamellae (yellow arrow). Movie S3 shows four consecutive tomograms of these disks. A 3D model obtained from segmentation is shown in Fig. 2*D*.

In another example, images from three *z*-planes of a cat rod photoreceptor are shown in Fig. 2 *E–G*. Three nascent disks are shown, one of which appears as little more than an elongated vesicle (red arrow). However, following this vesicle through different *z*-planes of the tomogram (Movie S4) reveals that it is continuous with the plasma membrane (yellow arrow in Fig. 2*G*). The resulting model from segmentation of the tomogram illustrates the 3D structure of this membrane structure and its connection to the plasma membrane. It represents a slightly flattened tubule that may have resulted from an invagination of the plasma membrane (arrows in Fig. 2*H*).

Nascent Disk Initiation. Analyses of the basal-most folding of the plasma membrane in tomograms from cat, mouse, and monkey rod OSs revealed a variety of structures similar to the structure illustrated in Fig. 2*H*. One example is shown from a tomogram of a monkey rod (Fig. 3 *A–C*). The model created by segmentation of that tomogram (Fig. 3 *D* and *E* and Movie S5) shows one of these structures that appears bilobed (arrows, Fig. 3*D*). Because these are always the basal-most structures associated with disk formation, they invariably occur in a thickened area of the connecting cilium, and can manifest various degrees of lateral expansion from their innermost region.

These observations suggest that disk morphogenesis may be initiated by an invagination of the plasma membrane that helps shape a membrane lamella and then contributes to the initiation of disk rim formation as the invagination expands laterally. Distal to this initiation structure, the membrane appears as a series of lamellae, with the more distal lamellae extending further outward (e.g., Fig. 3*A*), indicating the presence of outward

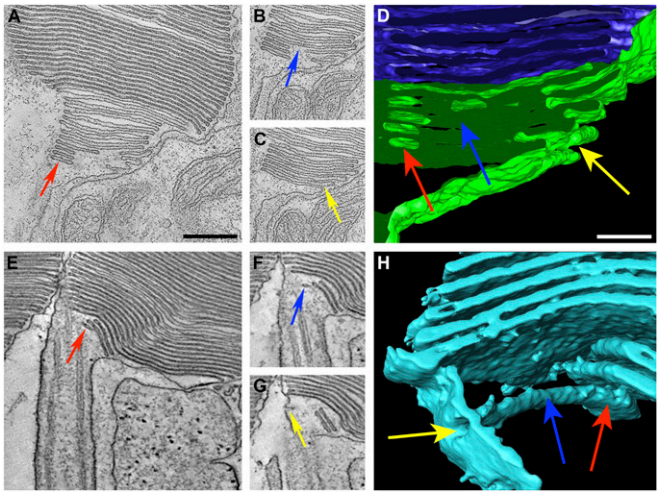

Fig. 2. Continuity of nascent disks with the plasma membrane. (*A–D*) Monkey. (*E–H*) Cat. *A–C* and *E–G* show different *z*-plane images from tomograms of the basal disks of rod OSs. Basal disks appear enclosed in one plane of section (red arrow in *A* and *E*), but are actually open to the extracellular space in another plane of section (yellow arrows in *C* and *G*). *D* and *H* show 3D renderings of the membrane structures. The arrows (red, blue, and yellow) indicate corresponding areas in the *z*-plane images (*A–C* and *E–G*) and the respective 3D models (*D* and *H*). (Scale bars: 250 nm in *A*; 100 nm in *D*.) *A–C* and *E–G* are at the same magnification, as are *D* and *H*.

growth, or an evagination process (which can be rather uneven, as illustrated in Fig. 2 *A–D*).

Closure of the Nascent Disks (Lamellae) by Rim Completion. Steinberg et al. (10) proposed that the basal lamellae become internalized as the disk rim is completed around the space between two adjacent lamellae. Analyses of our tomograms support this view, as illustrated in the example of selected *z*-planes and 3D modeling of a tomogram of a mouse rod (Fig. 3 *F–J* and Movie S6). In Fig. 3*F*, the 12 basal-most disks appear more dilated than the mature distal disks, a characteristic previously identified in basal lamellae in frog rod photoreceptors (19). In this *z*-plane, the three disks above the red arrow appear to be enclosed by the plasma membrane but still show the dilated morphology, whereas the other nine disks (red arrow and below) appear open. In a different *z*-plane, the fourth most distal disk appears enclosed (yellow arrow, Fig. 3*H*). In a *z*-plane intermediate to those shown in Fig. 3 *F* and *H*, the tip of this fourth disk appears to be in contact with the enveloping plasma membrane (blue arrow, Fig. 3*G*). In a 3D model created from segmentation of this tomogram (Fig. 3*I*), the point of contact can be seen as a transition zone between an area that is open (above the lamella indicated by the red arrow, and to the left of the blue arrow) and an area that is enclosed by the plasma membrane (to the right of the blue arrow). The blue arrow indicates what appears to be the leading edge of a disk rim forming from right to left. The dilated appearance of disks enclosed in a single *z*-plane by the plasma membrane suggests that these indeed are not mature disks, but represent lamellar outgrowths that are transitioning into mature disks; that is, the process of rim formation and plasma membrane growth is incomplete, leaving a small opening to the extracellular space.

Calycal Process of Mouse Rod Photoreceptors. Calycal processes arising from the inner segment and surrounding the base of the OS are a generally accepted feature of photoreceptors in most vertebrates, notwithstanding a recent claim that they are absent in mice (20). Tomographic data from the base of mouse rod OSs revealed that they indeed have a single, tongue-like calycal process opposite the connecting cilium. This process is evident as an extension from the inner segment to the right of the nascent disk and more distal disks in single *z*-planes (Fig. 3 *F–H*) and in the 3D visualizations of segmented tomograms (Fig. 3 *I* and *J* and Movie S7).

Nascent Disks on a Daily Cycle. The rate of addition of new disks to frog rod OSs varied greatly according to a daily cycle, with the number of open discs increasing threefold during the first 8 h of light in comparison with the dark portion of the light/dark cycle (21). Such cyclic variation also may help explain the controversy surrounding open and closed nascent disks in mammals. Consequently, we recorded the number of basal lamellae (open nascent disks) in monkey and mouse rods at different times of the day. Although lamellae were evident at all times sampled in both species, the number increased during the first part of the light period in monkey rods, similar to that reported for frog rods (21), but decreased during the same period in mouse rods (Fig. 4), suggesting a possible relationship with the diurnal and nocturnal habits of monkey and mouse, respectively.

Discussion

By ET of rod photoreceptor nascent disks from different species and using various fixation techniques, we have been able to address issues of disk membrane formation in an approach not taken in previous studies. The tomographic data allowed us not only to create very-high-resolution *z*-axis images (3–4 nm) of the nascent disk-forming region, but also to create high-resolution 3D models from the data. Previous studies, which typically relied on 2D images of ∼70-nm sections, have reported conflicting interpretations of nascent disk organization and thus mature disk formation. Our ET analyses of 300-nm sections showed that the nascent disks are continuous with the ciliary plasma membrane (thereby classified as lamellae), and appear to form by expansion of the plasma membrane. Our results also indicate novel information with regard to disk initiation.

Early TEM studies of mammalian retinas found that the disk membranes of cone photoreceptors and the basal disk membranes of rod photoreceptors are continuous with the ciliary plasma membrane (22–24). These observations led to the hypothesis that new disks are formed by invaginations of the ciliary plasma membrane (9). Steinberg et al. (10) also found that the nascent OS disks are continuous with the ciliary plasma membrane, but concluded that the growth of the disk membranes occurs through an evagination rather than an invagination. Importantly, that study also proposed the formation of the disk rim as the final growth stage. Studies of frog photoreceptors not only found that the nascent disks are amplifications of the plasma membrane (19), but also were able to label the nascent disks using Lucifer yellow as an extracellular tracer, demonstrating that they are open to the extracellular space (25).

Relatively recently, Sung and colleagues (11, 16) reported that the nascent disks of mouse rods are completely internal and proposed models of disk morphogenesis in which the disks form by expansion of the vesicular membrane. They argued that data for the earlier, open disk models came from tissue that was inadequately fixed, and postulated that the use of a mixture of formaldehyde and acrolein preserves disk membranes closer to their native state. However, although acrolein, a monoaldehyde introduced for TEM by Luft (26), has an advantage of rapid tissue penetration, its use has been limited because of reports that it solubilizes membranes (27). In addition, the idea that ordered membrane lamellae would form as artifacts from vesicles seems unlikely. It is noteworthy that in images of the HPF-FS samples (Fig. 1*B*) and also some of the conventionally processed samples (e.g., Fig. 1 *A* and *D*), the surfaces of neighboring lamellae appear very close to each other, with a spacing that resembles the intradisk space of the mature disks, which has been

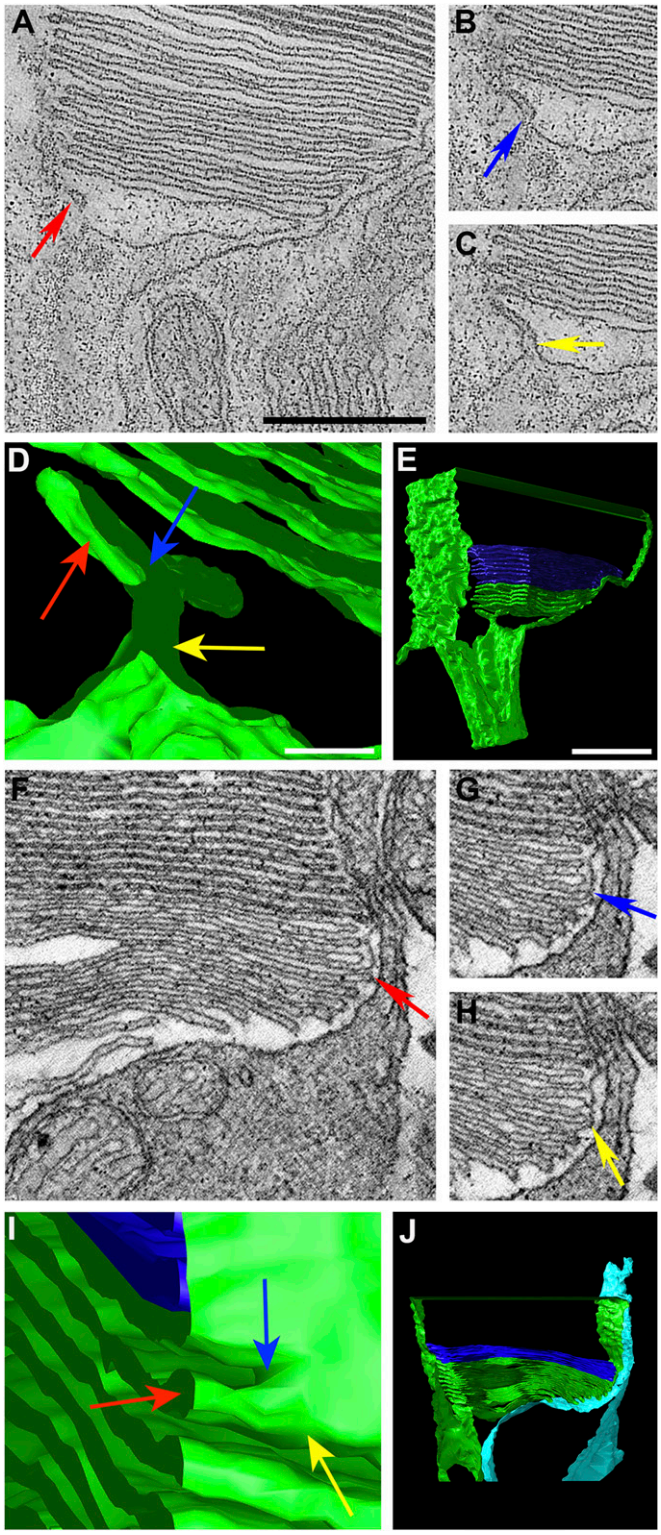

Fig. 3. EM tomography of nascent disk initiation and rim formation in monkey (*A–E*) and mouse (*F–J*). (*A–C*) Different *z*-plane images from a tomogram of monkey rod OS basal disks showing different profiles of a membrane structure (red, blue, and yellow arrows) that appears as a bilobed invagination in 3D renderings (*D* and *E*). *E* is from Movie S5; plasma membrane is green, mature disks are dark blue. (*F–H*) Different *z*-plane images from a tomogram of mouse rod OS basal disks. Arrows indicate the location of rim formation; below the arrows, the nascent disks appear as lamellae, and above them, they appear enclosed by the plasma membrane. (*I*) 3D rendering of a view from outside the cell. The space above the most mature lamella (red arrow) is partially closed (to the right of the blue arrow); to the left of the blue arrow, this space is still open. (*J*) Lower-magnification view of the 3D model. The inner segment and a calycal process (light blue) have been modeled separately from other plasma membrane (green). *J* is a frame of Movie S7. (Scale bars: 250 nm in *A*; 50 nm in *D*; 500 nm in *E*.) *A–C* and *F–H* are at the same magnification, as are *D* and *I*, and *E* and *J*.

measured as ∼4 nm (28). This observation indicates that the growing lamellae already have the highly ordered character of mature disk membranes. Moreover, the proximity of the adjacent lamellar surfaces may be sufficient to result in a force that drives the smaller lamella outward, following its more mature, distal neighbor (29).

Species difference may play a role in the controversy, considering that the rate of disk formation varies by species (30). However, different studies that used mouse retinas have reported both open (15) and closed (16, 17, 31) disks, suggesting that species difference alone does not provide a satisfactory explanation for the various observations. Nevertheless, to address the possibility of different results related to differences in species and fixation methodology, we tested three different mammalian species, as well as different methods for the preservation of mouse photoreceptors, including the use of HPF-FS.

Rapid freezing of cells provides a much faster preservation than chemical fixation. HPF is particularly advantageous for tissues, because it suppresses ice crystal formation, and, compared with freezing at ambient pressure, permits the freezing of much larger samples (32, 33). A recent study of the ultrastructure of the cilia and striated rootlets of mouse rods by cryo-ET used plunge-freezing of a purified OS suspension (31). Although that study provided novel ultrastructural detail, tomograms were limited to a very small *z*- axis depth, which compromised the extent of 3D segmentation. When combined with FS, HPF results in material that can withstand the extensive high-voltage exposure required in the substantial *z*-axis imaging for ET (34); however, the amount of tissue that can be preserved even by HPF is quite limited (up to 0.2–0.5 mm thick), necessitating previous dissection, during which cells can become damaged. Here, to stabilize the retina before dissection for HPF-FS, we used a brief cardiac perfusion with Karnovsky's fixative. With accessible cells, such as those in cell culture, this approach has been shown to generate tissue preservation close to that achieved by HPF-FS alone (18). Chemical fixation followed by HPF-FS is considered superior to conventional aldehyde fixation methods because it avoids the subsequent ambient temperature processing steps (18), during which lipids may be extracted (35). This conclusion is consistent with the linear, parallel profiles that we obtained of mouse OS disks prepared by HPF-FS, but not by chemical fixation alone (Fig. 1 *A* and *B*). Importantly, however, we did not observe any difference with respect to whether nascent disks were open or closed between rod OSs fixed and processed by HPF-FS and those fixed by perfusion with Karnovsky's fixative and processed by conventional TEM methods.

Our results with the three different mammalian species are largely consistent with the model of disk morphogenesis proposed by Steinberg et al. (10). In that model, nascent disks are continuous with the ciliary plasma membrane, at least in some region around their perimeter. Their increase in width associated with a more distal position is consistent with growth out from the axoneme, that is, growth by evagination. A significant difference in our data are reflected by the more detailed organization at the most basal part of the disk stack that we were able to obtain by ET. Here, *invaginations* of varied shapes appear in a bulge of the ciliary plasma membrane, suggesting that the initiation of a new lamella begins with a bulge and then an invagination of the ciliary plasma membrane. We propose that this invagination is important

CELL BIOLOGY

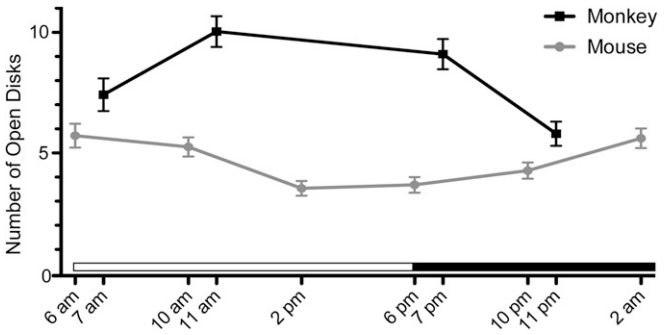

Fig. 4. Number of open disks throughout the daily cycle at the base of monkey and mouse rod OSs. Error bars indicate ± SD. The probability of no significant difference among the different times of day was determined by ANOVA to be < 0.001 for each species.

for generating the flattened organization of a lamella, and the lateral expansion of the innermost surface of the invagination (closest to the axoneme) initiates the circumferential processes that become the disk rim (Fig. 5 *A* and *B*). Subsequent outward growth of the lamella (Fig. 5*C*) is followed by completion of the disk rim (Fig. 5*D*), and resulting enclosure of the space between the lamellae to create a mature disk completely enclosed by the plasma membrane (Fig. 5*E*). A mature disk is thus formed from the adjacent membranes of two lamellae and contains what was originally extracellular space (Fig. 5); as noted above, the very small space between two adjacent lamellae appears similar to that between the two membranes of a mature disk. It has been shown that the initiation of new disks, but not the growth of the evaginations, requires f-actin (36, 37), so that membrane invagination, a critical first step in the process, may be dependent on an actin mechanism.

Whether the nascent disks are open or closed is also important with respect to other aspects of photoreceptor cell biology and electrophysiology. As the disk membranes are formed, critical sorting or at least maintenance of a separation of membrane proteins must occur. Within the disk membranes themselves, rim proteins (e.g., PRPH2, ROM1, ABCA4) are separated from proteins that will occupy the disk surfaces (e.g., RHO). In addition, proteins that function in the plasma membrane (e.g., the cGMP channel subunit proteins, such as CNGA1) must be separated from discrete disk membranes (12). ImmunoEM and trafficking studies of PRPH2 have shown that this protein is delivered to the cilium separately from RHO (38), and that it is not included in the most basal disks of rod OS (36, 39), consistent with an open lamellar structure for the basal disks. The presence of PRPH2 in the OS coincides only with rim formation (39, 40). CNGA1 appears to be trafficked directly to the rod OS plasma membrane, distal to the nascent disk region (36).

The early receptor potential (ERP), first reported by Brown and Murakami (41), appears to be generated by the movement of charge within each rhodopsin molecule as it changes its conformation on photobleaching. However, because the ERP occurs across the plasma membrane, only rhodopsin molecules that are in the plasma membrane can contribute to it. The signal from mammalian rods is too large to be explained without a subset of disks being open to the extracellular space, thus increasing the effective rhodopsin content of the plasma membrane (13). If the nascent disks are open, they could contribute to the ERP; if not, some of the mature rod disks must be exposed to the extracellular space, an observation not reported in any study to date.

The focus of the present study was on the organization of the nascent disks of rod photoreceptors. An additional observation made during the study merits comment because of a recent report indicating that mouse photoreceptors do not have calycal processes (20). In our *z*-stack of images from the tomograms of mouse OSs, we were able to identify the presence of a calycal process opposite the connecting cilium. A similar single calycal process has been shown in rat rod photoreceptors (39, 42).

Materials and Methods

Animals and Sample Preparation. C57BL/6J mice were housed at University of California, Los Angeles and used at age 6 wk. Adult cat, *Felis catus*, and rhesus monkey, *Macaca mulatta*, tissues were from previous studies performed at University of California, Santa Barbara, and University of California, San Francisco (43, 44). All animals were kept on a 12-h light/12-h dark cycle, and treated in accordance with appropriate institutional guidelines. Mouse retinas were fixed by immersion of posterior eyecups in 2% (vol/vol) formaldehyde and 2.5% (vol/vol) glutaraldehyde in 0.1 M phosphate buffer, or by transcardiac perfusion for 30 min with the same fixative.

For conventional TEM, eyecups were postfixed in 1% OsO_4 in 0.1 M cacodylate buffer for 1 h, dehydrated, and embedded in Araldite 502. Retinal tissue for HPF-FS was dissected after 5 min of cardiac perfusion with 50 mL of fixative, and small pieces (~1 mm × 1 mm × 0.2 mm) were placed in specimen carriers, transferred to a sample holder, and frozen in a Leica EM PACT2 high-pressure freezer. Samples were then placed in cryosubstitution medium containing 1% OsO_4 and 0.1% uranyl acetate in acetone within an automatic freeze substitution unit (EM AFS2; Leica). The temperature was raised slowly for 88 h to room temperature, while the fixative gradually replaced the water in the sample. Samples were then washed in acetone and propylene oxide, and embedded in Araldite 502. Cat and monkey tissue was fixed using transcardiac perfusion, as described previously (43, 44).

For conventional TEM, ~70-nm sections were stained with 5% (vol/vol) uranyl acetate and 0.4% lead citrate. Serial sections of 300-nm thickness were collected for ET on formvar-coated copper slot grids, and stained with 10% uranyl acetate in methanol and 0.4% lead citrate. In addition, sections were labeled with 15- and 20-nm colloidal gold fiducials on the top and the bottom of each grid, respectively, to aid the alignment of images in each tilt series.

ET Methods. ET was performed with an FEI Technai TF20, operated at 200 kV. Images were recorded using a 16-megapixel CCD camera (TVIPS) at original magnifications between 14,500× and 19,000×. Serial sections were imaged using double-tilt axis tomography with Batch Tomography software (FEI). The series were recorded with an underfocus of ~−5 μm from −70° to +70° along two tilt axes, with 2° increments at the lower tilt angles (range ±40°) and 1° increments above +40° and below −40°. To obtain the dual tilt

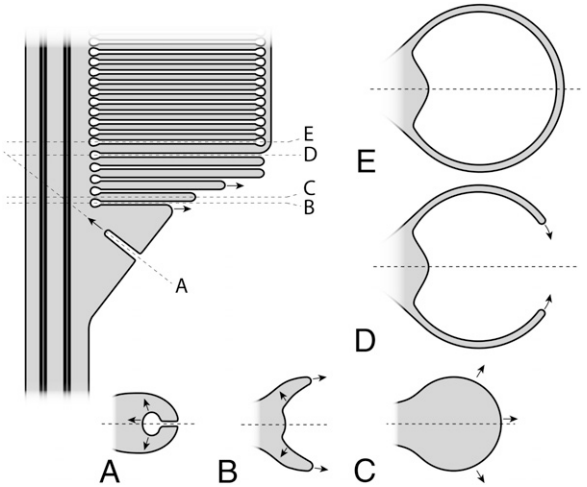

Fig. 5. Diagram of the organization of the nascent disks of a rod OS. Horizontal sections at different locations of the vertical section are shown. (*A*) An invagination that appears to initiate flattening of a protrusion of the ciliary plasma membrane. (*B*) Lateral expansion of the invagination (arrows in *A*), leading to the beginning of rim growth (arrows). (*C*) Lamella growth outward. (*D* and *E*) Growth of the rim leading to the enclosure of extracellular space between two adjacent lamellae (*D*), and thus the formation of a mature disk that is discrete from the plasma membrane (*E*).

datasets, the grid was rotated by 90° after the acquisition of a single tilt axis, and a second tilt series was recorded in the same location.

Data Processing. The images acquired in each tomography tilt series were aligned and combined to generate a tomographic reconstruction of the imaged 300-nm section using eTomo (IMOD). Fiducial-based alignment was used. After separate tomographic reconstructions were generated, tomograms from serial sections were joined into one volume along the *z*-axis, using the "join serial tomograms" function of eTomo, which runs a series of programs, including the interactive program *MIDAS* for alignment as well as programs for joining. Segmentation and subsequent image processing were conducted using 3dmod (bio3d.colorado.edu/imod/). In tomograms acquired from monkey and mouse, the membrane structures at the base of the rod OS were traced in every 3–10 *z*-slices to create a 3D model. Different regions of the photoreceptor were modeled as separate, enclosed objects. The OS plasma membrane, disk lamellae, and ciliary plasma membrane were modeled as one object and the inner segment plasma membrane was modeled as another object, even though all these membranes are continuous.

Segmentation and subsequent image processing of cat tomograms were conducted using Amira version 5.2.0 (FEI). Segmentation was based on distinct characteristics of the data; regions of interest (ROI) were selected, and data within the ROI were displayed using the "thresholding" and "smoothing" functions. Different colors represent separate membrane compartments. Movies of 3D models were generated using the Chimera interactive visualization program (University of California San Francisco), and movies of tilt series and tomogram reconstructions were generated using 3dmod (IMOD) and Fiji (National Institutes of Health), an open source processing package based on ImageJ.

Open Disk Quantification. To obtain the number of open disks at multiple time points throughout the day, electron micrographs of well-aligned rod OSs that included a longitudinal section of the axoneme were obtained from mouse and monkey retinas that had been prepared for conventional TEM. The number of observable open disks was counted on the side opposite the axoneme in 15–28 rod photoreceptors from several sections from one animal for each time of day. Variation by time of day was analyzed by ANOVA.

ACKNOWLEDGMENTS. We greatly appreciate the advice and help provided by Xinran Liu (Yale University) at the start of this project, and the valuable discussions on membrane properties with Wayne Hubbell (University of California, Los Angeles) and Jacob Israelachvili (University of California, Santa Barbara), and on the rod ERP with Gordon Fain (University of California, Los Angeles). We thank Luke Chang for some technical assistance, and we acknowledge the use of instruments at the Electron Imaging Center for Nanomachines, supported by the University of California, Los Angeles, and by an instrumentation grant from the National Institutes of Health (S10RR23057). This work was supported by National Institutes of Health Grants EY013408, EY024667, EY000331, and GM071940.

1. Besharse JC, Horst CJ (1990) The photoreceptor connecting cilium: A model for the transition zone. *Ciliary and Flagellar Membranes*, ed Bloodgood RA (Plenum, New York), pp 409–431.
2. Young RW (1967) The renewal of photoreceptor cell outer segments. *J Cell Biol* 33(1): 61–72.
3. Williams DS (2002) Transport to the photoreceptor outer segment by myosin VIIa and kinesin II. *Vision Res* 42(4):455–462.
4. Papermaster DS, Schneider BG, Besharse JC (1985) Vesicular transport of newly synthesized opsin from the Golgi apparatus toward the rod outer segment: Ultrastructural immunocytochemical and autoradiographic evidence in *Xenopus* retinas. *Invest Ophthalmol Vis Sci* 26(10):1386–1404.
5. Deretic D, Papermaster DS (1991) Polarized sorting of rhodopsin on post-Golgi membranes in frog retinal photoreceptor cells. *J Cell Biol* 113(6):1281–1293.
6. Sanyal S, Jansen HG (1981) Absence of receptor outer segments in the retina of *rds* mutant mice. *Neurosci Lett* 21(1):23–26.
7. Cohen AI (1983) Some cytological and initial biochemical observations on photoreceptors in retinas of *rds* mice. *Invest Ophthalmol Vis Sci* 24(7):832–843.
8. Yang Z, et al. (2008) Mutant prominin 1 found in patients with macular degeneration disrupts photoreceptor disk morphogenesis in mice. *J Clin Invest* 118(8):2908–2916.
9. Nilsson SE (1964) Receptor cell outer segment development and ultrastructure of the disk membranes in the retina of the tadpole (*Rana pipiens*). *J Ultrastruct Res* 11: 581–602.
10. Steinberg RH, Fisher SK, Anderson DH (1980) Disc morphogenesis in vertebrate photoreceptors. *J Comp Neurol* 190(3):501–508.
11. Sung CH, Chuang JZ (2010) The cell biology of vision. *J Cell Biol* 190(6):953–963.
12. Molday RS, Molday LL (1987) Differences in the protein composition of bovine retinal rod outer segment disk and plasma membranes isolated by a ricin-gold-dextran density perturbation method. *J Cell Biol* 105(6 Pt 1):2589–2601.
13. Woodruff ML, Lem J, Fain GL (2004) Early receptor current of wild-type and transducin knockout mice: photosensitivity and light-induced $Ca2^+$ release. *J Physiol* 557(Pt 3): 821–828.
14. Volland S, Esteve-Rudd J, Hoo J, Yee C, Williams DS (2015) A comparison of some organizational characteristics of the mouse central retina and the human macula. *PLoS One* 10(4):e0125631.
15. Carter-Dawson LD, LaVail MM (1979) Rods and cones in the mouse retina, I: Structural analysis using light and electron microscopy. *J Comp Neurol* 188(2):245–262.
16. Chuang JZ, Zhao Y, Sung CH (2007) SARA-regulated vesicular targeting underlies formation of the light-sensing organelle in mammalian rods. *Cell* 130(3):535–547.
17. Chakraborty D, Conley SM, Al-Ubaidi MR, Naash MI (2014) Initiation of rod outer segment disc formation requires RDS. *PLoS One* 9(6):e98939.
18. Sosinsky GE, et al. (2008) The combination of chemical fixation procedures with high-pressure freezing and freeze substitution preserves highly labile tissue ultrastructure for electron tomography applications. *J Struct Biol* 161(3):359–371.
19. Besharse JC, Hollyfield JG, Rayborn ME (1977) Turnover of rod photoreceptor outer segments, II: Membrane addition and loss in relationship to light. *J Cell Biol* 75(2 Pt 1): 507–527.
20. Sahly I, et al. (2012) Localization of Usher 1 proteins to the photoreceptor calyceal processes, which are absent from mice. *J Cell Biol* 199(2):381–399.
21. Besharse JC, Hollyfield JG, Rayborn ME (1977) Photoreceptor outer segments: Accelerated membrane renewal in rods after exposure to light. *Science* 196(4289): 536–538.
22. Sjöstrand FS (1959) The organization of membrane layers. *Rev Mod Phys* 31:301–318.
23. Moody MF, Robertson JD (1960) The fine structure of some retinal photoreceptors. *J Biophys Biochem Cytol* 7:87–92.
24. Dowling JE (1967) The organization of vertebrate visual receptors. *Molecular Organization and Biological Function*, ed Allen JM (Harper & Row, New York).
25. Matsumoto B, Besharse JC (1985) Light and temperature modulated staining of the rod outer segment distal tips with Lucifer yellow. *Invest Ophthalmol Vis Sci* 26(5): 628–635.
26. Luft JH (1959) The use of acrolein as a fixative for light and electron microscopy. *Anat Rec* 133:305.
27. Glauert AM (1975) Fixation, Dehydration and Embedding of Biological Specimens (North-Holland, Amsterdam).
28. Nickell S, Park PS, Baumeister W, Palczewski K (2007) Three-dimensional architecture of murine rod outer segments determined by cryoelectron tomography. *J Cell Biol* 177(5):917–925.
29. Israelachvili JN (2011) *Intermolecular and Surface Forces* (Academic, Oxford, UK), 3rd Ed.
30. Pearring JN, Salinas RY, Baker SA, Arshavsky VY (2013) Protein sorting, targeting and trafficking in photoreceptor cells. *Prog Retin Eye Res* 36:24–51.
31. Gilliam JC, et al. (2012) Three-dimensional architecture of the rod sensory cilium and its disruption in retinal neurodegeneration. *Cell* 151(5):1029–1041.
32. Dahl R, Staehelin LA (1989) High-pressure freezing for the preservation of biological structure: Theory and practice. *J Electron Microsc Tech* 13(3):165–174.
33. Studer D, Graber W, Al-Amoudi A, Eggli P (2001) A new approach for cryofixation by high-pressure freezing. *J Microsc* 203(Pt 3):285–294.
34. McDonald KL, Auer M (2006) High-pressure freezing, cellular tomography, and structural cell biology. *Biotechniques* 41(2):137–143, 139, 141 passim.
35. Korn ED, Weisman RA (1966) I: Loss of lipids during preparation of amoebae for electron microscopy. *Biochim Biophys Acta* 116(2):309–316.
36. Nemet I, Tian G, Imanishi Y (2014) Submembrane assembly and renewal of rod photoreceptor cGMP-gated channel: Insight into the actin-dependent process of outer segment morphogenesis. *J Neurosci* 34(24):8164–8174.
37. Williams DS, Linberg KA, Vaughan DK, Fariss RN, Fisher SK (1988) Disruption of microfilament organization and deregulation of disk membrane morphogenesis by cytochalasin D in rod and cone photoreceptors. *J Comp Neurol* 272(2):161–176.
38. Tian G, et al. (2014) An unconventional secretory pathway mediates the cilia targeting of peripherin/rds. *J Neurosci* 34(3):992–1006.
39. Arikawa K, Molday LL, Molday RS, Williams DS (1992) Localization of peripherin/rds in the disk membranes of cone and rod photoreceptors: Relationship to disk membrane morphogenesis and retinal degeneration. *J Cell Biol* 116(3):659–667.
40. Molday RS, Hicks D, Molday L (1987) Peripherin: A rim-specific membrane protein of rod outer segment discs. *Invest Ophthalmol Vis Sci* 28(1):50–61.
41. Brown KT, Murakami M (1964) A new receptor potential of the monkey retina with no detectable latency. *Nature* 201:626–628.
42. Kessel RG, Kardon RH (1979) Nervous tissue—eye and ear. *A Text Atlas of Scanning Electron Microscopy*, ed Kessel RG (WH Freeman, San Francisco).
43. Anderson DH, Fisher SK (1979) The relationship of primate foveal cones to the pigment epithelium. *J Ultrastruct Res* 67(1):23–32.
44. Fisher SK, Steinberg RH (1982) Origin and organization of pigment epithelial apical projections to cones in cat retina. *J Comp Neurol* 206(2):131–145.